Surface Phenomena of Deuterized Ethanol Exposed Zircaloy-4 Surfaces

Juyun Park, Se-Won Jung, Mi-Sun Chun, and Yong-Cheol Kang*

*Department of Chemistry, Pukyong National University, Busan 608-737, Korea. *E-mail: yckang@pknu.ac.kr*
Received April 18, 2009, Accepted May 4, 2009

We report the results of the surface chemistry of deuterized ethanol exposed Zircaloy-4 (Zry-4) surfaces with various amount of C_2D_5OD exposures at 190 K. This system was examined with Auger electron spectroscopy (AES) and temperature programmed desorption (TPD) techniques. In TPD study, D_2 was evolved at two different desorption temperature regions accompanying with broad desorption background. The lower temperature feature at around 520 K showed first-order desorption kinetics. The high temperature desorption peak at around 650 K shifted to lower desorption temperature as the exposure of C_2D_5OD increased. The Zr(MNV) Auger peak shifted about 2.5 eV from 147 eV to lower electron energy followed by 300 L of C_2D_5OD dosing. This implies metallic zirconium was oxidized by deuterized ethanol adsorption. After stepwise annealing of the oxidized Zry-4 sample up to 843 K, the shifted Zr(MNV) peak was gradually shifted back to metallic zirconium peak position. After the sample was heated to 843 K, the oxygen content near the Zry-4 surface was recovered to clean surface level. The concentration of carbon, however, was not recovered by annealing the sample.

Key Words: Auger electron spectroscopy, Zircaloy-4, Ethanol. Temperature programmed desorption

Introduction

Due to the low thermal neutron capture cross-section, good corrosion resistance, and adequate mechanical properties, Zircaloy-4 (Zry-4) is often chosen as cladding tube materials in nuclear industry.[1,2] Zry-4 contains 1.4 wt% Sn, 0.23 wt% Fe, 0.1 wt% Cr, and Zr as the balance component. Zry-4 has been of great concern and investigated with a variety of surfaces in many fields. The corrosion,[3-9] oxidation,[10-17] and hydrogen absorption kinetics[18-23] of Zry-4 and its nuclear application have been reported in literatures. Zry-4 oxidation by water (H_2O) and steam has been reported in many studies.[24-32] Ramsier's group reported that heating H_2O/Zry-4 surface resulted in molecular desorption of water at both low and high temperatures. Also they investigated that the behavior of water with sulfur dioxide pre-exposed Zry-4 surface.[27] They studied that adsorption of SO_2 caused shift of the Zr(MNN) Auger electron feature by 3.0 eV, while subsequent water adsorption attenuated the sulfur Auger signal and resulted in the development of a zirconium oxide. The effects of adsorbates on the oxidation of Zry-4 in air and steam were studied by the measurement of the weight gain of specimens.[28]

Reaction of alcohols on transition metal surfaces are of great interest. Ethanol has been receiving considerable attention recently because of its high potential for producing molecular hydrogen to power fuel cells.[33-36] Ethanol is attractive due to its renewable nature since it can be produced in high yield by fermentation of crops. Because ethanol can be easily transported on board hydrogen generation by reforming is an attractive solution to feed fuel cells. Despite a few papers have studied about interaction of C_2D_5OD on zirconium, the surface chemistry of ethanol dosed on Zry-4 surface is not well known yet. We report here the results of the thermal effect on the surface chemistry of C_2D_5OD dosed Zry-4 surface using TPD and AES techniques.

Experimental Section

The Zry-4 sample used in this study has a thickness of 1.70 mm and surface area of 9.35 mm × 9.55 mm in a rectangular shape. It was prepared through many steps of polishing with different meshes of abrasive papers and mechanical polisher (Buehler, gamma alumina, 0.05 micron) for the final step of surface polishing. Then the polished Zry-4 was rinsed with acetone in ultrasonic cleaner for ten minutes. After the sample was rinsed with acetone and then the surface was blown with dry nitrogen gas. The prepared Zry-4 sample was mounted on the custom designed sample holder by spot welding on Ta wires. The type-K thermocouple was spot welded on the side of the Zry-4 for monitoring temperature. Before the experiment was performing, the sample was cleaned by many cycles of Ar^+ (99.999% purity, Aldrich) sputtering followed by annealing to 843 K. During the Ar^+ sputtering process (IES 5, Omicron), the pressure of Ar^+ was kept at 1.5×10^{-5} Torr for 1 hour in order to make 20 μA of a target current. And the Ar^+ fluence was 5.1×10^{23} Ar^+/cm^2 per sputtering cycle. Cleanliness of the sample was confirmed by AES.

For TPD experiments, the sample was facing to the quadrupole mass spectrometer (QMS: Dycor Dymaxion, AMETEK) and the sample temperature was increased at a rate of 1 K/s by resistive heating using a feedback PID controller. The temperature of the sample was monitored by type-K thermocouple spot welded on the side of Zry-4 sample. The sample was cooled down by liquid nitrogen. When the temperature of the sample reached about 190 K, Zry-4 was exposed to the gas phase C_2D_5OD with various exposures. In order to identify the hydrogen produced from the ethanol not from the residual hydrogen the analysis chamber, high purity deuterized ethanol was introduced. The C_2D_5OD (99.5%, atom %) was purified through several times of freeze-pump-thaw (FPT) methods before introducing it into UHV chamber. The purity of C_2D_5OD after several cycles of FPT was checked by QMS. After the sample

was cooled down to 190 K. C_2D_5OD was backfilled into the main analysis chamber through a precision leak valve kept the pressure at 1.0×10^{-6} Torr during gas dosing and the exposure time was measured until the pressure reached to 5.0×10^{-9} Torr, then the sample was linearly heated up to 843 K. The possible desorption species from the deuterized ethanol adsorbed Zry-4 surfaces, such as H_2, HD, D_2, H_2O, D_2O, CO, and CD_3O were monitored applying multiple ion monitoring (MIM) mode in QMS.

The base pressure of UHV analysis chamber was kept at low 10^{-10} Torr range. The details of the UHV analysis chamber are described elsewhere.[37-39] The electron beam energy at 3 keV was used for retarding field AES (SpectaLEED 4-Grid, Omicron). The AES experiments were performed with 140 μA of a beam current, 0.3 mA of an emission current, 1.17 A of a filament current, and 75 μA of a target current. The survey scan range for AES applied in this work was from 5 to 600 eV. The parameters for AES survey scan were 1 eV of an energy step, 3 mV of a lock-in sensitivity, and 100 ms of a lock-in time constant. The high resolution AE spectra were taken at the ranges for zirconium, carbon, and oxygen were from 70 to 180 eV, 240 to 300 eV, and 280 to 540 eV, respectively, with 0.2 eV of energy step and other factors were kept the same as survey scan. In AES study, sample temperature was raised stepwisely from 190 K up to 503, 628, 653, 753, and 843 K then cooled down the sample to adsorption temperature for investigation of thermal effect on the C_2D_5OD/Zry-4 system. These temperatures were chosen in according to the results of TPD experiment. After sample was cooled down, AES data were collected.

Results and Discussion

Figures 1 (a) and (b) show the representative thermal desorption spectra of 2 amu (H_2^+ or D^-) and 4 amu (D_2^+), respectively, after different C_2D_5OD exposures at 190 K of adsorption temperature. The gas exposures are presented by langmuir (1 L = 1.0×10^{-6} Torr·s) unit. When the exposure of gas was lower than 50 L, no noticeable desorption was observed. Even ultra pure deuterized ethanol was used for this study hydrogen exchange could be occurred in the gas handling line. Because of the hydrogen exchange, H_2 desorption peak was detected. The hydrogen (2 amu) thermal desorption peak was observed at around 660 K at 53 L of ethanol exposure which increased in intensity with increasing C_2D_5OD exposure. The desorption peak temperature shifted to lower temperature according to the increase of gas exposure. This phenomenon could be explained by the second-order desorption kinetics. Especially, note the D_2 evolution (Figure 1 (b)), the desorption peaks appeared both ~520 K and ~650 K overlapped with broad desorption background from ~300 K to 750 K. This broad desorption background implies that complicate desorption kinetics was involving in D_2 desorption. The peak position of low temperature desorption feature (520 K) was constant with increasing the exposures of adsorbate indicating that the desorption of D_2^+ was the first-order desorption verified by peak-shape analysis. The high temperature desorption feature (660 K) gradually increased in intensity with exposure and shifted to lower temperature. It could indicate the second-order desorption kinetics.

The desorption feature of D_2 at low temperature was almost saturated at 53 L of C_2D_5OD exposure but the feature at high temperature was grown at the exposure increased (Fig. 1(b)). This could be explained that the low temperature feature was developed by the deuterium existed near the zircaloy-4 surface region which was easily saturated by 53 L of exposure and the other was evolved by the deuterium stayed in the bulk region. Higher exposure of C_2D_5OD, higher concentration of deuterium in the bulk is. The high temperature feature was only detected in H_2 desorption because the hydrogen existed in the bulk before C_2D_5OD exposure was desorbed (Fig. 1(a)).

Figure 2 shows the AES survey spectra of C_2D_5OD/Zry-4 system with various annealing temperatures. The intensity of Zr(MNV) Auger peak decreased after C_2D_5OD dosing on Zry-4 and then increased by annealing the sample as we expected. When the sample was annealed to higher tempera-

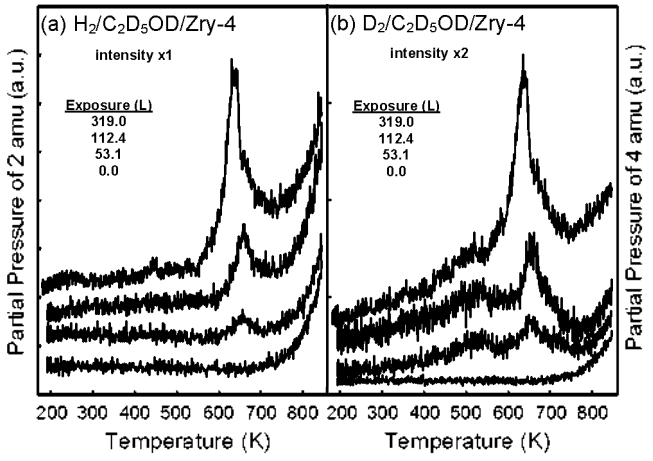

Figure 1. Temperature programmed desorption spectra of (a) 2 amu and (b) 4 amu following C_2D_5OD adsorption on Zircaloy-4 at 190 K. The numbers in the figure represent the exposure in langmuir unit (L). The notations used in the title of these figures, such as H_2/C_2D_5OD/Zry-4, means H_2 evolution after C_2D_5OD dosed on the Zry-4 surfaces.

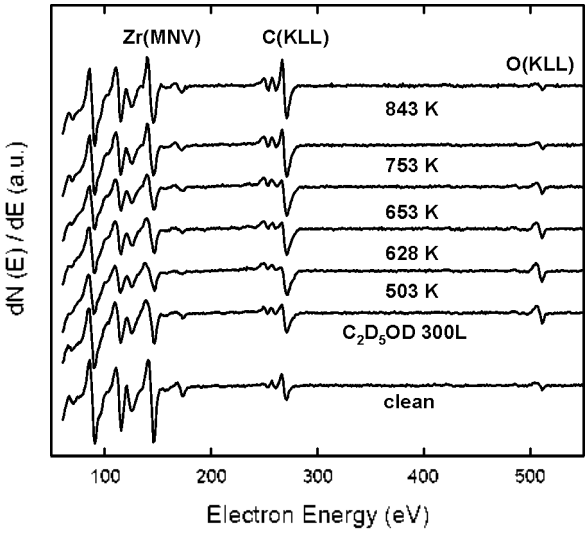

Figure 2. Survey Auger electron spectra of the C_2D_5OD dosed Zry-4 surfaces.

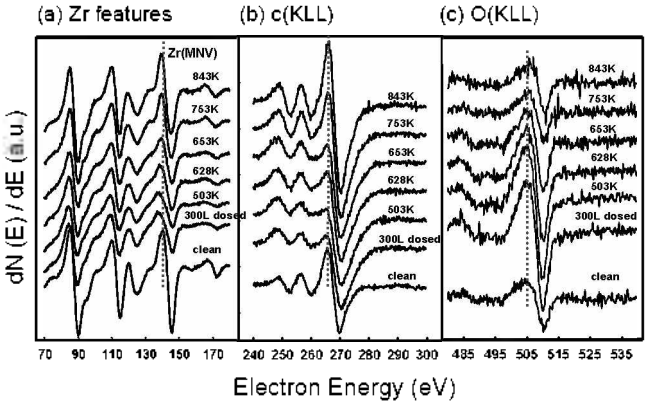

Figure 3. (a) High resolution Auger electron spectra of the Zr features including Zr (MNV, 147 eV). (b) AES of the C (KLL, 270 eV) peak and (c) AES spectra of the O (KLL, 510 eV) peak. The vertical lines are put on the peak maximum position of the clean surface for clarity of peak shifting.

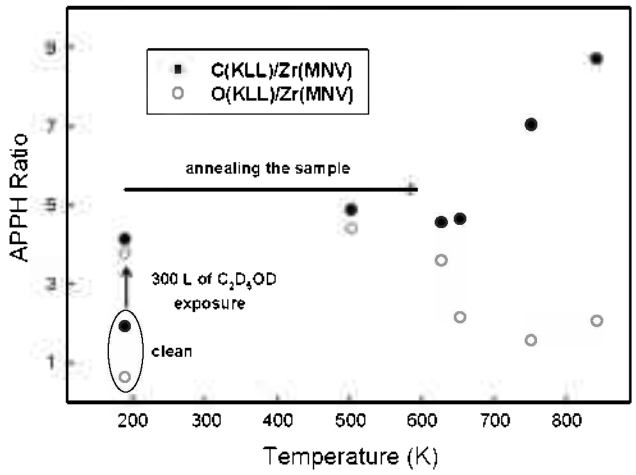

Figure 4. Auger peak-to-peak heights (APPH) ratio versus annealing temperature. Filled circles represent for C(KLL)/Zr(MNV) and open circles represent for O(KLL)/Zr(MNV). The data inside of the circle bottom of the left in the figure present APPH ratios of C/Zr and O/Zr of the clean Zry-4 surface.

ture, the intensity of O(KLL) Auger peak decreased but that of C(KLL) increased. To study the details of the surface chemistry, high resolution AES experiments were carried out for the energy ranges of Zr(MNV), C(KLL), and O(KLL).

Figures 3 (a), (b), and (c) show the high resolution AE spectra of zirconium, carbon, and oxygen regions, respectively. We collected AE spectra after stepwise annealing of the sample to our interested temperatures which were chosen considering with the TPD spectra shown in Figures 1, at and after the desorption peak maximum. The peak positions of Zr(MNV), C(KLL), and O(KLL) are assigned at the electron kinetic energy of 147, 270, and 510 eV, respectively. The vertical lines in the figures added for clarity. The intensity of Zr(MNV) feature was decreased after 300 L of C_2D_5OD exposure and gradually recovered by annealing as we expected. We should notice in Figure 3 (a) that the Zr(NMV) AE feature shifted to lower electron energy region (~2.5 eV) than the original peak position followed by C_2D_5OD dosing then shifted back to higher electron energy by increasing the temperature of annealing. This implies that the oxidation state of zirconium changed from metallic zirconium to zirconium oxide then back to nearly metallic zirconium by annealing. The change of zirconium oxidation state was supported by the AE spectra of oxygen (Figure 3 (c)) as well. As we can see in Figure 3 (c), the O(KLL) peak was increased by 300 L of C_2D_5OD exposure. Then the intensity of O(KLL) was decreased by annealing to the level before dosing of C_2D_5OD. The Auger electron intensity of C(KLL) stayed almost constant until the sample temperature reached to 628 K shown in Figure 3 (b). After this temperature C(KLL) intensity increased by annealing. This could be happened that the defragmented carbon in subsurface region was diffused out after the constituents near the surface were desorbed out to vacuum by annealing. These carbon diffused from the subsurface region was not cleaned before 10 cycles of Ar sputtering process. We should notice that the line shape of C(KLL) shown in Figure 3 (b). The line shape of C(KLL) feature, *i.e.* oscillation of peak at low kinetic energy side, could be used to differentiate carbidic and graphitic carbon reported by Gomer's group.[40] The peak oscillation of low kinetic energy region of C(KLL) was diminished when the sample was annealed to 503 K, then the oscillation was recovered with further annealing the sample to 843 K. This implies that the dominant carbon state of the C_2D_5OD/Zry-4 changed from carbidic through graphitic to carbidic carbon on the surface by annealing. Tanaka *et al.* have reported the formation of hybrid surface of carbide and graphite layers at 630-640 K on Ni surface by disproportion reaction of CO.[41] Further study needs to verify the carbon state by work function measurement for this system.

Figure 4 shows the Auger peak-to-peak height (APPH) ratios of C(KLL, 270 eV)/Zr(MNV, 147 eV) and O(KLL, 510 eV)/Zr(MNV). The APPH ratios of C/Zr and O/Zr are 1.91 and 0.62, respectively for the clean surface. The APPH ratios are calculated concerning with Auger sensitivity factors of the elements. The both ratios are increased after 300 L of deuterized ethanol dosing, and nearly stayed in constant level until the sample was heated to 628 K. When the sample was heated over 653 K, the ratio of C/Zr increased gradually but that of O/Zr decreased nearly back to the clean surface level. The carbon diffused onto the surface region by heating formed carbide form with zirconium, because of its small diffusion coefficient.[42] The diffused out surface oxygen with large diffusion coefficient could be diffused into the bulk caused relatively lower surface contents of oxygen than that of carbon. These phenomena is consistent with the observation reported by other group.[43,44]

Conclusions

The surface chemistry of C_2D_5OD on Zry-4 surface was investigated using AES and TPD methods. Isotopic hydrogen was detected from deuterized ethanol dosed Zry-4 surfaces at two different desorption temperature regions accompanying with broad desorption background. This shows the possibility of using hydrocarbon derivatives for the source of hydrogen used in fuel cell. The lower temperature feature at around 520 K stayed the same temperature increasing C_2D_5OD exposure.

This implies D_2 desorption is first-order desorption kinetics. The TPD peak of D_2 at around 650 K was shifted to lower desorption temperature as the exposure of C_2D_5OD increased. In AES study, the Zr(MNV) Auger peak was shifted about 2.5 eV from 147 eV to lower electron energy followed by 300 L of C_2D_5OD dosed. This implies metallic zirconium was oxidized by deuterized ethanol adsorption then reduced back to metallic zirconium by annealing because the oxygen near the surface was depopulated by heat treatment.

Acknowledgments. This work was supported by the Korea Research Foundation Grant funded by the Korean Government (MOEHRD) (KRF-2006-331-C00146).

References

1. Ha, Y. K.; Han, S. H.; Park, S. D.; Park, Y. S.; Kim, W. H. *Chemical Interaction between UO_2 Fuel and Zircaloy Clad*; Korea Atomic Energy Research Institute: Report KAERI/AR-697/2004.
2. Wilson, P. D. *The Nuclear Fuel Cycle: From Ore to Wastes*; Oxford University Press: New York, 1996; p 89.
3. Ravi Shankar, A.; Raju, V. R.; Narayana Rao, M.; Kamachi Mudali, U.; Khatak, H. S.; Raj, B. *Corr. Sci.* **2007**, *49*, 3527.
4. Sundaram, C. V. *T. Indian I. Metals* **1986**, *39*, 12.
5. Yao, M. Y.; Zhou, B. X.; Li, Q.; Liu, W. Q.; Geng, X.; Lu, Y. P. *J. Nucl. Mater.* **2008**, *374*, 197.
6. Wan, Q.; Bai, X.; Zhang. X. *Mater. Res. Bull.* **2006**, *41*, 387.
7. Kim, W.; Jung, K. S.; Choi, B. H.; Kwon, H. S.; Lee, S. J.; Han, J. G.; Guseva, M. I.; Atamanov, M. V. *Surf. Coat. Technol.* **1995**, *76*, 595.
8. Chen, X. W.; Bai, X. D.; Deng, P. Y.; Peng, D. Q.; Chen, B. S. *Nucl. Instr. and Meth. B* **2003**, *211*, 512.
9. Liu, X.; Bai, X.; Zhou, C.; Wei, L. *Surf. Coat. Technol.* **2004**, *182*, 138.
10. Abolhassani, S.; Dadras, M.; Leboeuf, M.; Gavillet, D. *J. Nucl. Mater.* **2003**, *321*, 70.
11. Bozzano, P. B.; Ipohorski, M.; Versaci, R. A. *Acta Microscopica* **2004**, *13*, 47.
12. Hofmann, P. *J. Nucl. Mater.* **1999**, *270*, 194.
13. Moulin, G.; El Tahhan, R.; Favergeon, J.; Viennot, M.; Berger, P. *Mater. Sci. Forum.* **2006**, *522-523*, 425.
14. Bai, X. D.; Wang, S. G.; Xu, J.; Bao, J.; Chen, H. M.; Fan, Y. D. *J. Nucl. Mater.* **1998**, *254*, 266.
15. Li, J.; Bai, X.; Zhang, D.; Li, H. *Appl. Surf. Sci.* **2006**, *252*, 7436.
16. Stojilovic, N.; Ramsier, R. D. *J. Nucl. Mater.* **2006**, *350*, 163.
17. Berger, P.; El Tahhann, R.; Moulin, G.; Viennot, M. *Nucl. Instr. and Meth. B* **2003**, *210*, 519.
18. Takagi, I.; Hashizumi, M.; Yamahami, A.; Maehara, K.; Higashi, K. *J. Nucl. Mater.* **1997**, *248*, 306.
19. Steinbrück, M. *J. Nucl. Mater.* **2004**, *334*, 58.
20. Meyer, G.; Kobrinsky, M.; Abriata, J. P.; Bolcich, J. C. *J. Nucl. Mater.* **1996**, *229*, 48.
21. Gómez, M. P.; Domizzi, G.; López Pumarega, M. I.; Ruzzante, J. E. *J. Nucl. Mater.* **2006**, *353*, 167.
22. Kim, S. J.; Kim, K. H.; Baek, J. H.; Choi, B. K.; Jeong, Y. H.; Jung, Y. H. *J. Nucl. Mater.* **1998**, *256*, 114.
23. Fernández, G. E.; Meyer, G.; Peretti, H. A. *J. Alloys & Compd.* **2002**, *330*, 483.
24. Tupin, M.; Pijolat, M.; Valdivieso, F.; Soustelle, M.; Frichet, A.; Barberis, P. *J. Nucl. Mater.* **2003**, *317*, 130.
25. Kim, J. H.; Lee, M. H.; Choi, B. K.; Jeong, Y. H. *J. Nucl. Mater.* **2007**, *362*, 36.
26. Kim, J. H.; Lee, M. H.; Choi, B. K.; Jeong, Y. H. *Nucl. Eng. Des.* **2005**, *235*, 67.
27. Stojilovic, N.; Ramsier, R. D. *Appl. Surf. Sci.* **2006**, *252*, 5839.
28. Park, K. H.; Cho, Y. C.; Kim, Y. G. *J. Nucl. Mater.* **1999**, *270*, 154.
29. Stojilovic, N.; Ramsier, R. D. *Surf. Interface Anal.* **2006**, *38*, 139.
30. Hong, H. S.; Moon, J. S.; Kim, S. J.; Lee, K. S. *J. Nucl. Mater.* **2001**, *297*, 113.
31. Bai, X.; Xu, J.; He, F.; Fan, Y. *Nucl. Instr. and Meth. B* **2000**, *160*, 49.
32. Stojilovic, N.; Bender, E. T.; Ramsier, R. D. *J. Nucl. Mater.* **2006**, *348*, 79.
33. Sheng, P. Y.; Bowmaker, G. A.; Idriss, H. *Appl.Catalysis A; General* **2004**, *261*, 171.
34. Silva, A. M.; BArandas, A. P. M. G.; Costa, L. O. O.; Borges, L. E. P.; Nattoso, L. V.; Noronga, F. B. *Cata. Today* **2007**, *129*, 297.
35. Barthos, R.; Széchenyi, A.; Koós, Á.; Solymosi, F. *Appl. Catal. A: Gen.* **2007**, *327*, 95.
36. Sheng, P. Y.; Chiu, W. W.; Yee, A.; Norrison, S. J.; Idriss, H. *Catal. Today* **2007**, *129*, 313.
37. Kwon, J. H.; Youn, S. W.; Kang, Y. C. *Bull. Korean Chem. Soc.* **2006**, *27*, 11.
38. Oh, K. S.; Kang, Y. C. *Bull. Korean Chem. Soc.* **2007**, *28*, 1341.
39. Jung, H. Y.; Kang, Y. C. *Bull. Korean Chem. Soc.* **2007**, *28*, 1751.
40. Whitten, J. E.; Gomer, R. *Surf. Sci.* **1996**, *347*, 280.
41. Nakamura, J.; Hirano, H.; Xie, M.; Matsuo, I.; Yamada, T.; Tanaka, K. *Surf. Sci.* **1989**, *222*(1,2), L809.
42. Foord, J. S.; Goddard, P. J.; Lambert, R. M *Surf. Sci.* **1980**, *94*, 339.
43. Stojilovic, N.; Weber, D. W.; Ramsier, R. D. *Appl. Surf. Sci.* **2003**, *218*, 188.
44. Stojilovic, N.; Farkas, N.; Ramsier, R. D. *Appl. Surf. Sci.* **2008**, *254*, 2866.